Dyes and Pigments 156 (2018) 291–298

Contents lists available at ScienceDirect

Dyes and Pigments

journal homepage: www.elsevier.com/locate/dyepig

Mechanofluorochromic properties of aggregation-induced emission-active tetraphenylethene-containing cruciform luminophores

Yonghui Wang[a,1], Defang Xu[b,1], Huaizhi Gao[a], Ying Wang[a], Xingliang Liu[a,*], Aixia Han[a], Chao Zhang[a], Ling Zang[c,**]

[a] Chemical Engineering College, Qinghai University, Xining 810016, China
[b] State Key Laboratory of Plateau Ecology and Agriculture, Qinghai University, Xining 810016, China
[c] Department of Materials Science and Engineering, University of Utah, Salt Lake City, UT 84108, USA

ARTICLE INFO

Keywords:
Cruciform
Tetraphenylethene
Intramolecular
Charge-transfer
Aggregation-induced
Emission
Mechanofluorochromism

ABSTRACT

Two twisted donor–acceptor cruciform luminophores (**DHCS-TPE** and **DMCS-TPE**) that were composed of two π-conjugated segments connected via a central benzene core have been prepared. Such cruciforms showed unique intramolecular charge transfer (ICT) emission, obvious aggregation-induced emission (AIE) properties (α_{AIE} = 19 and 20, respectively) and high solid state efficiency (0.913 and 0.424, respectively). Especially, the two compounds exhibited substituent-dependent mechanofluorochromic (MFC) behavior. The as-prepared powders of the more twisted **DMCS-TPE** could emit strong blue-green light centered at 474 nm, and the fluorescence color changed into yellowish green (531 nm) after grinding, a red shift of 57 nm was observed. Such mechanochromism was reversible upon the treatment of grinding and fuming with DCM. The high contrast MFC behavior of **DMCS-TPE** originated from the planarization of the molecular conformation and subsequent planar intramolecular charge transfer (PICT) under external force. By sharp contrast, the less twisted **DHCS-TPE** exhibited no MFC behavior. The reason is that the less twisted molecular conformation of **DHCS-TPE** generates strong intermolecular forces and close packing. Thus compared to **DMCS-TPE**, the crystalline solid powders of **DHCS-TPE** possess higher lattice energy and better structural stability. The grinding of the crystalline solid powders of **DHCS-TPE** cannot lead to amorphization and mechanochromic luminescence.

1. Introduction

The development of mechanofluorochromic (MFC) materials [1] that change their solid-state emission color in response to external force stimuli (such as grinding, pressing, shearing, deformation, etc.) remains an interesting but challenging subject because such materials not only possess significance in fundamental research but also have potential applications in memory devices [2], sensors [3], security inks [4] and optoelectronic devices [5]. Up to now, there has been an increasing interest in the design and characterization of MFC materials including tetraphenylethene [6], 9,10-divinylanthracene [7], triphenylacrylonitrile [5c,8] and organoboron complexes [9,10]. Nevertheless, MFC materials possessing high solid-state luminescence efficiency and an obvious color contrast are still rare. The main reason is that many organic luminescent dyes usually exhibit strong fluorescence in dilute solution, and most of their emissions become weak or thoroughly quenched in solid or aggregation states due to the ACQ effect [11]. To overcome this problem, developing aggregation-induced emission (AIE) luminophore, which was first discovered by Tang and co-workers in 2001 [12], is a rational and promising choice. Generally, AIE molecules possess the strongly twisted conjugated backbones, which can hinder intermolecular close stacking and intense π–π interaction to probably endow such materials with strong solid emission and MFC behavior. And a number of AIE fluorophores have been found to be promising MFC materials [6,7a-c,10,13]. However, creating such organic AIE MFC materials, which combine high contrast mechanofluorochromism, excellent reversibility, and high solid-state fluorescence efficiency, is still strikingly desirable. Thus, great attention should be paid to the design and synthesis of new AIE MFC luminophores, in particular, based on novel frameworks, with high emission in the solid states.

Cruciform fluorophores, which are donor- and/or acceptor-functionalized cross-shaped chromophores with an aromatic ring as the common π-center, have gained an increasing interest owing to their potential applications in chemosensors [14], organic light-emitting

* Corresponding author.
** Corresponding author.
E-mail addresses: liuxl1219@163.com (X. Liu), lzang@eng.utah.edu (L. Zang).
[1] These authors contributed equally to this work.

https://doi.org/10.1016/j.dyepig.2018.04.021
Received 22 December 2017; Received in revised form 30 March 2018; Accepted 13 April 2018
Available online 14 April 2018
0143-7208/

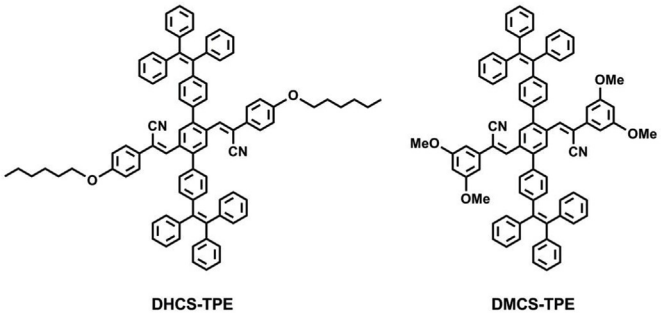

Scheme 1. The molecular structures of **DHCS-TPE** and **DMCS-TPE**.

diodes (OLED) [15], nonlinear optical materials [16], and organic photovoltaic cells (OPVs) [17]. In these cruciforms, appropriate donor and acceptor substitution results in compounds possessing the frontier molecular orbitals (FMOs) spatially disjoint from one another; in these cases, the HOMO and LUMO localize on the crossed arms of the molecules. This spatial separation of FMOs endows the molecules with unique and interesting optical and optoelectronic properties. Herein, we successfully synthesized two twisted donor–acceptor cross-conjugated π-systems (**DHCS-TPE** and **DMCS-TPE**, Scheme 1) with two conjugation circuits intersecting at the central benzene core, and investigated the impact of molecular structure on photophysical properties from the perspective of electronic and steric effects. In the two cruciforms, one of the axes is donor (tetraphenylethene) substituted and the other axis is acceptor (cyanostyryl) substituted, and thus species with spatially separated FMOs could be attained. Moreover, the crowding in the central benzene forces the surrounding substituents to distort from the ring plane, resulting in effective depression of close packing and enhancement of emission quantum yields in the solid state. Results illustrated that both **DHCS-TPE** and **DMCS-TPE** exhibit strong ICT nature, significant AIE characteristics, high solid state efficiency, and substituent-dependent MFC behavior.

2. Experimental section

2.1. Materials and measurements

2.1.1. General

^{1}H and ^{13}C NMR spectra were recorded on a Bruker-Avance III (400 MHz) spectrometer by using $CDCl_3$ as the solvents. UV-visible spectra were obtained on a Shimadzu UV-2550 spectrophotometer. Fluorescence measurements were performed on a Cary Eclipse Fluorescence Spectrophotometer. The absolute fluorescence quantum yields for as-prepared solids of **DHCS-TPE** and **DMCS-TPE** were measured on an Edinburgh FLS920 steady state spectrometer using an integrating sphere. HRMS spectra were recorded on MALDI-TOF MS Performance (Shimadzu, Japan). Elemental analyses were performed with a Perkin-Elmer 240C elemental analyzer by investigation of C, H, and N. XRD patterns were obtained on a Bruker D8 Focus Powder X-ray diffraction instrument. The calculations for **DHCS-TPE** and **DMCS-TPE** were based on the density functional theory (DFT) and performed at the B3LYP/6-31G(d) level using the Gaussian 09W program package.

2.1.2. Preparation of the samples for AIE study

A stock solution of luminogen in THF with a concentration of 1.0×10^{-3} M was prepared. An aliquot (0.1 mL) of the stock solution was transferred to a 10 mL volumetric flask. After the appropriate amount of THF was added, distilled water was added slowly under sonication to give 1.0×10^{-5} M solution with different fractions of water. The PL measurement of the resultant solutions was performed immediately.

2.1.3. Preparation of the samples for mechanofluorochromism study

The ground powders were prepared by grinding the initial powders with a pestle and mortar. The fumed samples were obtained by fuming the ground powders with DCM for 2 min.

2.1.4. Materials

THF was distilled from sodium and benzophenone under nitrogen immediately prior to use. Ethanol was distilled under normal pressure over sodium under nitrogen before use. The other chemicals were used as received without further purification. Compound **2** was synthesized according to the literature [18].

2.2. Synthesis

2.2.1. 4,4″-bis(1,2,2-triphenylvinyl)-[1,1′:4′,1″-terphenyl]-2′,5′-dicarbaldehyde (3)

Compound **1** (4.00 g, 13.70 mmol), **2** (15.47 g, 41.11 mmol), Pd$(PPh_3)_4$ (200 mg, 0.173 mmol), Na_2CO_3 (8.00 g, 75.48 mmol) were added into toluene/H_2O (400 mL, v/v = 3/2). The mixture was heated to reflux under nitrogen atmosphere for 48 h. After cooling to room temperature, the resulting precipitate was collected by filtration, and dried under vacuum. The crude product was purified by column chromatography (silica gel, CH_2Cl_2), affording a light yellow solid (10.13 g), yield 93%. ^{1}H NMR (400 MHz, $CDCl_3$) δ 10.00 (s, 2H), 8.05 (s, 2H), 7.18–7.09 (m, 38H) (Fig. S17); ^{13}C NMR (100 MHz, $CDCl_3$) δ 191.87, 144.47, 144.24, 143.42, 143.37, 143.26, 142.06, 139.97, 137.87, 136.38, 134.24, 131.66, 131.34, 131.29, 129.97, 129.42, 129.04, 128.23, 127.85, 127.82, 127.72, 126.87, 126.71, 126.67, 125.31 (Fig. S18); HRMS (MALDI-TOF) *m/z*: $[M]^+$ Calcd for $C_{60}H_{42}O_2$ 794.3185; Found 794.3192 (Fig. S19). Anal. Calcd (%) for $C_{60}H_{42}O_2$: C 90.65, H 5.33; Found: C 90.58, H 5.41.

2.2.2. (2Z,2′Z)-3,3′-(4,4″-bis(1,2,2-triphenylvinyl)-[1,1′:4′,1″-terphenyl]-2′,5′-diyl)bis(2-(4-(hexyloxy)phenyl)acrylonitrile) (DHCS-TPE)

Compound **3** (1.50 g, 1.89 mmol) and **4** (1.23 g, 5.66 mmol) were added into dry ethanol (150 mL) and dry THF (15 mL), and then CH_3ONa (0.31 g, 5.74 mmol) was added quickly. The mixture was refluxed with stirring for 24 h under an atmosphere of nitrogen. After cooling to room temperature, the resulting precipitate was collected by filtration, and dried under vacuum. The crude product was purified by column chromatography (silica gel, CH_2Cl_2/petroleum ether, v/v = 2/1), affording a bright yellowish-green solid (1.62 g). Yield 72%. ^{1}H NMR (400 MHz, $CDCl_3$) δ 8.16 (s, 2H), 7.47 (d, J = 8.8 Hz, 4H), 7.35 (s, 2H), 7.26 (d, J = 10.8 Hz, 6H), 7.16–7.06 (m, 32H), 6.98 (d, J = 8.8 Hz, 4H), 4.05 (t, J = 6.4 Hz, J = 6.8 Hz, 4H), 1.88–1.81 (m, 4H), 1.54–1.48 (m, 4H), 1.41–1.37 (m, 8H), 0.94 (t, J = 6.8 Hz, J = 7.2 Hz, 6H) (Figs. S20 and S21); ^{13}C NMR (100 MHz, $CDCl_3$) δ 160.17, 143.66, 143.61, 143.54, 143.40, 141.57, 140.91, 140.41, 139.11, 136.97, 133.40, 131.50, 131.39, 131.32, 130.22, 129.41, 127.77, 127.68, 127.35, 126.60, 126.57, 126.38, 118.13, 115.03, 113.21, 68.29, 31.58, 29.16, 25.72, 22.62, 14.05 (Fig. S22); HRMS (MALDI-TOF) *m/z*: $[M]^+$ Calcd for $C_{88}H_{76}N_2O_2$ 1192.5907; Found 1192.5918 (Fig. S23). Anal. Calcd (%) for $C_{88}H_{76}N_2O_2$: C 88.55, H 6.42, N 2.35; Found: C 88.63, H 6.52, N 2.29.

2.2.3. (2Z,2′Z)-3,3′-(4,4″-bis(1,2,2-triphenylvinyl)-[1,1′:4′,1″-terphenyl]-2′,5′-diyl)bis(2-(3,5-dimethoxyphenyl)acrylonitrile) (DMCS-TPE)

By following the synthetic procedure for **DHCS-TPE**, **DMCS-TPE** was synthesized by using **3** (1.60 g, 2.01 mmol), **5** (1.07 g, 6.03 mmol) and CH_3ONa (0.33 g, 6.11 mmol) as the reagents. The crude product was purified by column chromatography (silica gel, CH_2Cl_2/petroleum ether, v/v = 3/2), affording a light yellow solid (1.68 g). Yield 75%. ^{1}H NMR (400 MHz, $CDCl_3$) δ 8.15 (s, 2H), 7.47 (s, 2H), 7.23 (d, J = 8 Hz, 4H), 7.14–6.99 (m, 34H), 6.72 (s, 4H), 6.54 (s, 2H), 3.86 (s, 12H) (Fig. S24); ^{13}C NMR (100 MHz, $CDCl_3$) δ 161.24, 143.81, 143.49, 143.45,

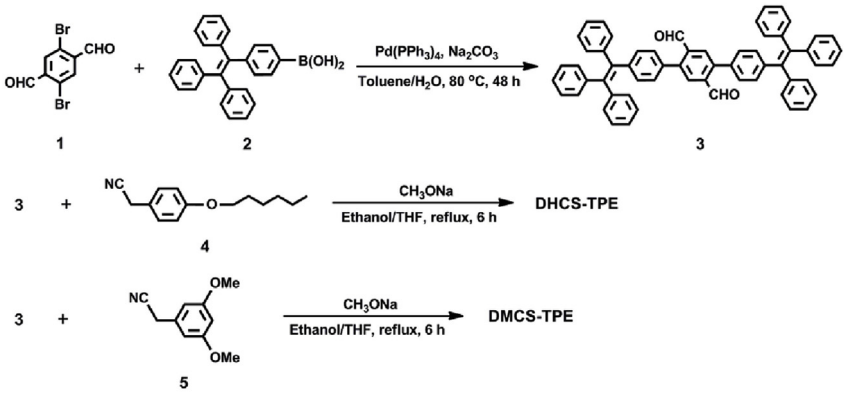

Scheme 2. Synthetic routes of **DHCS-TPE** and **DMCS-TPE**.

143.35, 141.93, 141.77, 141.26, 140.24, 136.68, 136.01, 133.40, 131.54, 131.35, 131.28, 130.39, 129.34, 127.78, 127.74, 127.65, 126.65, 126.59, 126.53, 117.85, 113.71, 104.49, 101.18, 55.52 (Fig. S25); HRMS (MALDI-TOF) *m/z*: $[M]^+$ Calcd for $C_{80}H_{60}N_2O_4$ 1112.4553; Found 1112.4568 (Fig. S26). Anal. Calcd. (%) for $C_{80}H_{60}N_2O_4$: C 86.30, H 5.43, N 2.52; Found: C 86.36, H 5.51, N 2.44.

3. Result and discussion

3.1. Synthesis of *DHCS-TPE* and *DMCS-TPE*

The synthetic routes for cruciform luminophores **DHCS-TPE** and **DMCS-TPE** are shown in Scheme 2. The key intermediate **3** was prepared by Suzuki-Miyaura coupling reaction between **1** and boric acid **2** catalyzed by $Pd(PPh_3)_4$ in toluene–H_2O in a high yield of 93%. The target molecules **DHCS-TPE** and **DMCS-TPE** were synthesized between **3** and substituted phenylacetonitriles **4** and **5** via standard Knoevenagel condensation in the presence of sodium methoxide, respectively, to give good yields of 72% and 75%. **DHCS-TPE** and **DMCS-TPE** are soluble in common organic solvents, such as $CHCl_3$, CH_2Cl_2, THF, benzene and toluene, but show poor solubility in alcohols and aliphatic hydrocarbon solvents, such as cyclohexane, hexane, methanol and ethanol. It is worth mentioning that we have tried to allow the condensation reaction between **3** and 2-(4-methoxyphenyl)acetonitrile, unfortunately, the product obtained had so poor solubility that it was not soluble in common organic solvents. Therefore, 2-(4-(hexyloxy)phenyl)acetonitrile was selected to react with **3**, which enabled the product **DHCS-TPE** to possess moderate solubility. All the intermediates and target molecules were characterized by ^1H and ^{13}C NMR, MALDI-TOF mass spectrometry, and C, H, N elemental analyses.

3.2. UV-vis absorption and fluorescent emission spectra in solutions

To investigate the solvent effect on the photophysical properties, the absorption and emission spectra of **DHCS-TPE** and **DMCS-TPE** were measured in various solvents, and the corresponding photophysical data were collected in Tables S1 and S2. As shown in Fig. 1a, for compound **DHCS-TPE**, in different solvents, it exhibited a strong major absorption peak at ca. 340 nm originating from π–π* transition and weak bands at the longer wavelength ca. 400 nm attributed to the CT transition between electron donor (tetraphenylethene unit) and electron acceptor (dicyanodistyrylbenzene axis) [19], which could be confirmed by the solvent-dependent emission spectra. Fig. 1c showed the solvent-dependent photoluminescence (PL) spectra of **DHCS-TPE**. It was found that the maximum emission bands of **DHCS-TPE** became broad and red-shifted significantly with increasing polarity of the solvent. For example, in cyclohexane, **DHCS-TPE** gave a strong emission band at 464 nm, but with the increasing solvent polarity, its emission band was red-shifted to 509 nm in DCM accompanied by emission bands broaden. Combined with the large Stokes shifts, the broadening and red-shift of the emission bands, we suggested that intramolecular charge-transfer (ICT) transitions of **DHCS-TPE** took place in more polar solvents [20]. And the longer wavelength emissions can be assigned to ICT emissions. Similarly, **DMCS-TPE** displayed the π–π* transition bands at ca. 330 nm and CT transition bands ca. 400 nm (Fig. 1b), and its emission spectra also showed the broadening and red-shift of the emission bands from cyclohexane to DCM (Fig. 1d), indicating an ICT character for the excited state. The effects of solvents on the emission features can be further evaluated by the relationship between the solvent polarity parameter (Δf) and Stokes shift ($\Delta\upsilon$) the absorption and emission maxima (Lippert – Mataga equation) [21,22]. Δf and $\Delta\upsilon$ of the two compounds in different solvents are listed in Tables S1 and S2. It was clear that both **DHCS-TPE** and **DMCS-TPE** showed positive solvatochromism. Their emission peaks red-shifted and quantum yields decreased gradually with the increasing of Δf. From the plots of $\Delta\upsilon - \Delta f$ (Fig. S1), we could find that the slopes of the fitting line for **DHCS-TPE** and **DMCS-TPE** were as high as 7448 and 14657, exhibiting significant solvatochromism effect. In addition, in the same solvent, the maximum ICT emission wavelength of **DHCS-TPE** was smaller than that of **DMCS-TPE**, indicating the ICT degrees of the two compounds in the excited state increased in a sequence of **DHCS-TPE** < **DMCS-TPE** [18,23], which were same as the order of the onset wavelength in absorption (Figs. S2–S7).

For better insight into the influence of the geometric and electronic structures of **DHCS-TPE** and **DMCS-TPE** on their photophysical properties, density functional theory (DFT) calculations were performed on the two compounds with the Gaussian 09W package. The geometrical structures are optimized at the at the B3LYP/6-31G(d) level. Fig. 2 shows the optimized molecular configuration and the electron distribution of the HOMOs and LUMOs for **DHCS-TPE** and **DMCS-TPE**. It is found that the LUMO densities for **DHCS-TPE** and **DMCS-TPE** are mainly distributed along the acceptor dicyanodistyrylbenzene axis. The HOMO densities for **DHCS-TPE** are located in the whole molecule, and in the case of **DMCS-TPE**, the HOMO densities were distributed in over the donor tetraphenylethene unit. The reason for the difference in the distribution of the HOMO densities for two molecules is below: the electron-donating ability of the alkoxy can weaken the electron-withdrawing ability of the acceptor dicyanodistyrylbenzene axis. And thus the electron-withdrawing ability of the acceptor dicyanodistyrylbenzene axis in **DHCS-TPE** is weaker than that of **DMCS-TPE** because the electron-donating ability of *para*-hexyloxy in **DHCS-TPE** is stronger than that of *meta*-methoxy in **DMCS-TPE**. As a result, the ICT would occur from the donor (tetraphenylethene) to the acceptor (dicyanodistyrylbenzene axis) for the excited state. Moreover, **DMCS-TPE** possesses larger CT degree in the excited state than that of **DHCS-TPE**. The above inference is consistent with the observed optical property. In addition, for **DHCS-TPE**, the dihedral angles between two vinyl planes and the central benzene are 28.1° and 32.6°, respectively. And dihedral

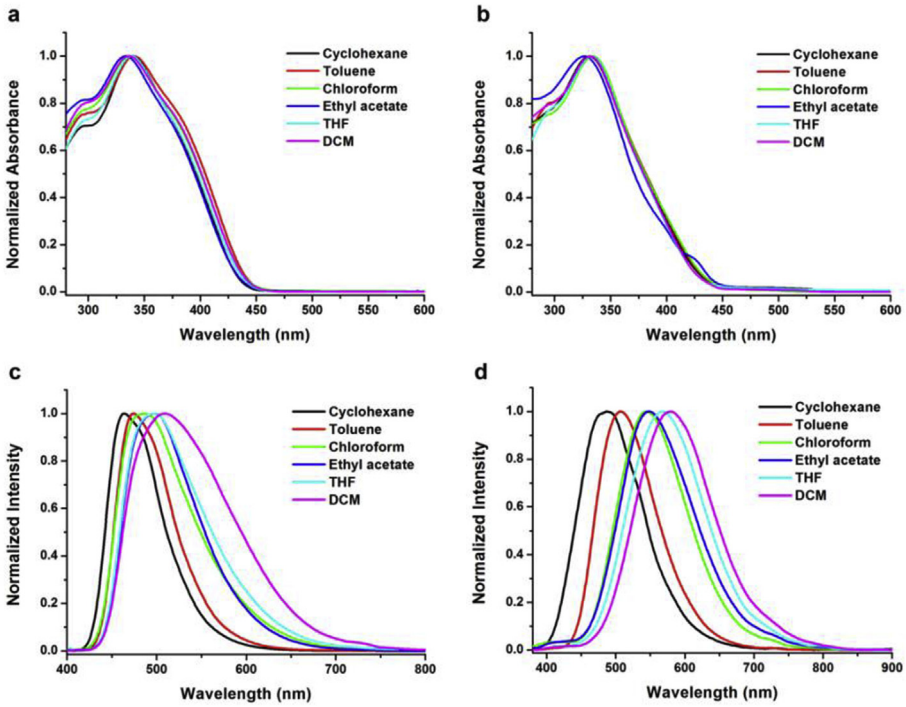

Fig. 1. Normalized UV-vis absorption spectra of **DHCS-TPE** (a) and **DMCS-TPE** (b), and normalized PL spectra of **DHCS-TPE** (c, λ_{ex} = 390 nm) and **DMCS-TPE** (d, λ_{ex} = 370 nm) in different solvents (1.0×10^{-5} mol L^{-1}).

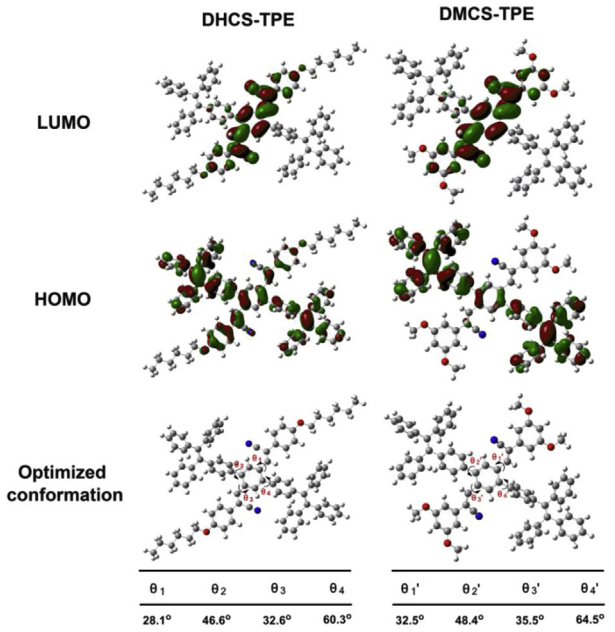

Fig. 2. Electron density distributions in the HOMO and LUMO states and optimized conformation of **DHCS-TPE** and **DMCS-TPE** calculated by DFT in Gaussian 09 at the B3LYP/6-31G(d) level.

angles between two side benzene rings and the central core are 46.6° and 60.3°, respectively. And for **DMCS-TPE**, the corresponding dihedral angles are 32.5°, 35.5°, 48.4° and 64.5°, which are larger than that of **DHCS-TPE**. Such high torsional angles should be ascribed to the steric hindrance between tetraphenylethene and substituted cyanostyryl groups. As a result, **DHCS-TPE** and **DMCS-TPE** show specially twisted conformation, which disfavors close molecular packing and π–π interactions in the solid state and this may endow them, especially **DMCS-TPE**, with solid state emission, AIE characteristics and MFC behavior.

3.3. Aggregation induced emission (AIE)

Tetraphenylethene (TPE) is a well-known AIE luminogen. So far, a large number of the molecules containing TPE unit have been developed for their simple synthetic routes and notable AIE performance [6]. When excited with 365 nm UV light, the as-prepared powders of **DHCS-TPE** and **DMCS-TPE** could emit strong green and blue-green light, respectively. However, relatively weak blue and yellow light was observed from their dilute THF solutions, revealing their AIE feature. To confirm the AIE nature of **DHCS-TPE** and **DMCS-TPE**, we measured their PL spectra in dilute mixtures of water–THF with different water fractions (f_w, the volume percentage of water in THF/water mixtures). Because the two compounds are insoluble in water and soluble in THF, increasing the water fraction in the mixed solvent could thus change their existing forms from a solution state in the pure THF to the aggregated particles in the mixtures with high water contents, thereby changing their PL spectra. As shown in Fig. 3, in pure THF, **DHCS-TPE** and **DMCS-TPE** could emit blue and yellow fluorescence with maxima at 493 and 561 nm, respectively, but the intensity was weak and Φ_f is only 0.049 and 0.021. When the proper amount of water is added into THF solution, the PL intensities initially decreased and the emission peaks show red shifts due to the increased solvent polarity. The fluorescence quenching is attributed to the ICT effect in polar solvent for **DHCS-TPE** and **DMCS-TPE** with D-A structures. As f_w is above 40% and 50%, the emission peaks were recovered and the PL intensities started to increase rapidly for the two luminogens, respectively, at which solvating powers of the mixtures are so worse that the luminogen molecules tend to aggregate, inside which the encapsulated the two luminogen molecules locate in a nonpolar environment and the ICT process is limited, thus the fluorescence is recovered, At a high f_w of 90%, the bright blue and yellow-green light emitting of **DHCS-TPE** and **DMCS-TPE** is observed for the aggregates, which is about 3 and 2 times higher than that in the pure THF, respectively. At the same time, the emission peaks of the two luminogens blue-shift from 515 (f_w = 40% for **DHCS-TPE**) and 583 nm (f_w = 50% for **DMCS-TPE**) to 484 and 520 nm, respectively. Thus, the increase in PL intensity could be attributed to the AIE effect derived from the formation of molecular aggregates when

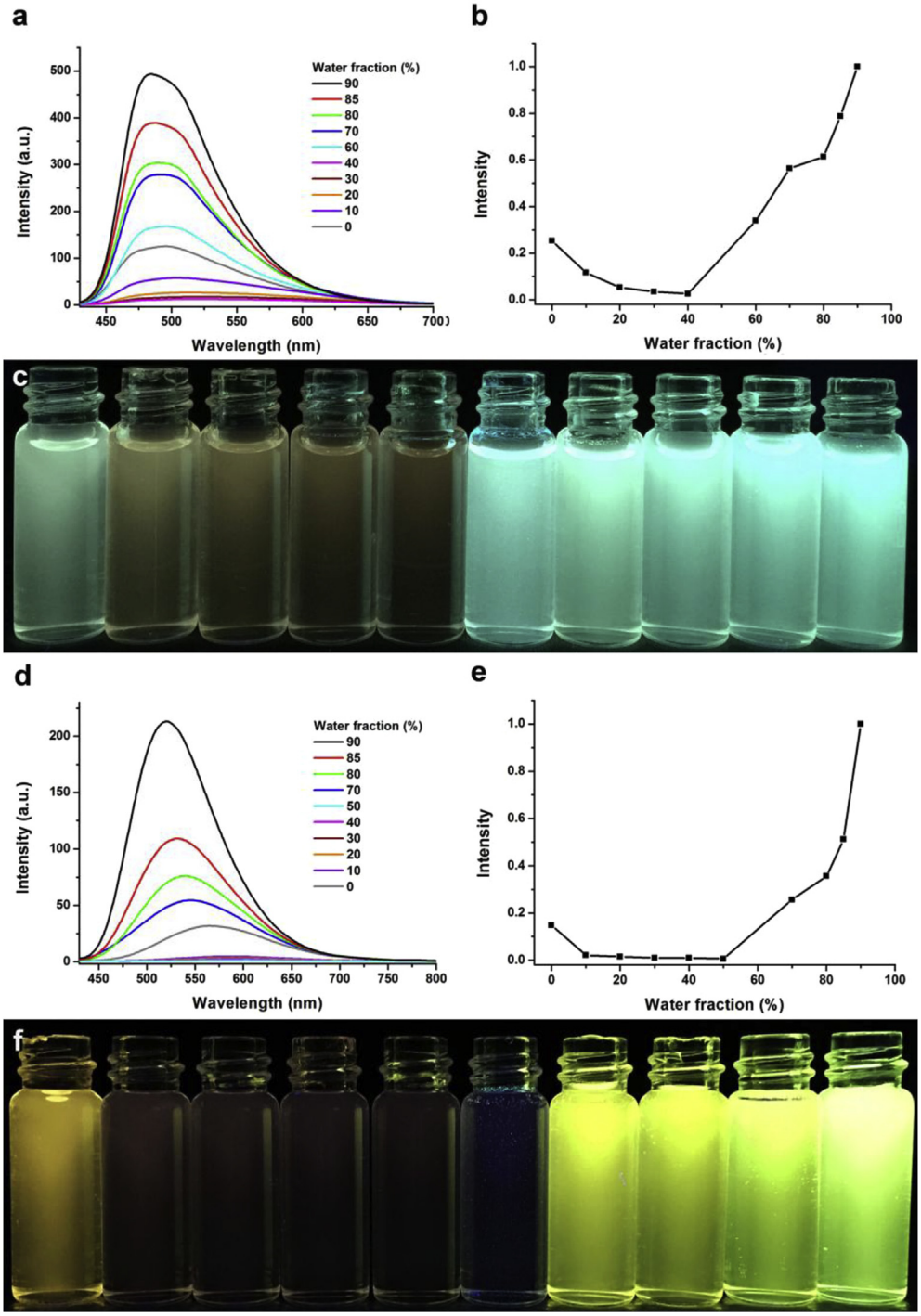

Fig. 3. PL spectra of **DHCS-TPE** ((a), λ_{ex} = 400 nm) and **DMCS-TPE** ((d), λ_{ex} = 370 nm) in THF/water mixtures with different f_w. Normalized fluorescence emission intensities of **DHCS-TP**E (b) and **DMCS-TPE** (e) in THF/water mixtures with different f_w. The fluorescence images of **DHCS-TPE** (c) and **DMCS-TPE** (f) with various water fractions (from 0% to 90%) under UV light (365 nm).

adding water to the solution. The aggregated particles obtained are characterized using dynamic light scattering (DLS) and shows the existence of nano-aggregates as their main constituent in the solvent mixtures with high water contents (Figs. S8 and S9). The AIE nature of **DHCS-TPE** and **DMCS-TPE** can also be further confirmed by the vivid contrast fluorescent images of the solvent mixtures from 0% to 90% (Fig. 3c and f).

To determine the reason for the AIE effect of **DHCS-TPE** and **DMCS-TPE**, the dependencies of the optical properties on solvent temperature were examined. With the decreasing of the system temperature, for the two compounds, their emission peaks red-shift and their fluorescence intensities increased in THF (Fig. S10). Because low-temperature environments can suppress molecular motions (such as torsion and vibration), which might be beneficial to extend the conjugate length of the molecules, and thus the red-shifts of the emission peaks and the enhancement of the PL intensities would occur. Therefore, the main reason for AIE of **DHCS-TPE** and **DMCS-TPE** could be attributed to be the restriction of intramolecular rotation (RIR) associated with the aromatic groups and decreased solvent polarity effect when molecules precipitate [10a,b]. To quantitatively evaluate the AIE effect of **DHCS-**

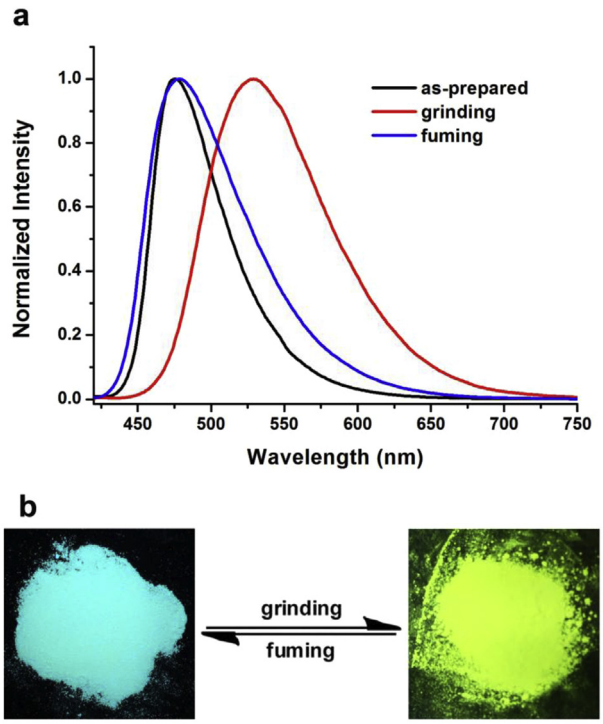

Fig. 4. (a) Normalized fluorescent spectra of **DMCS-TPE** in different solid-states: as-prepared, grinding and fuming (λ_{ex} = 410 nm). (b) Photographs of **DMCS-TPE** color changes under grinding and fuming stimuli. (For interpretation of the references to color in this figure legend, the reader is referred to the Web version of this article.)

TPE and **DMCS-TPE**, the fluorescence quantum yields of the luminogens in solution ($\Phi_{f,s}$) and as prepared solid ($\Phi_{f,aps}$) states were determined. The $\Phi_{f,aps}$ value for **DHCS-TPE** and **DMCS-TPE** is 0.913 and 0.424, respectively, which are considerably boosted compared to those in pure THF (0.049 and 0.021), giving AIE factors ($\alpha_{AIE} = \Phi_{f,aps}/\Phi_{f,s}$) of 19 and 20 with respect to those in THF.

3.4. Mechanofluorochromic (MFC) properties

As discussed above, the two luminogens **DHCS-TPE** and **DMCS-TPE** possessing the highly torsional molecular conformations, the AIE feature, ICT characteristics, and moreover high solid state efficiency, would be promising candidates as stimuli responsive smart materials [10]. To investigate whether the two luminogens **DHCS-TPE** and **DMCS-TPE** exhibit mechanochromic luminescence, their solid emission properties were studied. The fluorescence responses of **DMCS-TPE** toward grinding and fuming processes are illustrated in Fig. 4. Upon exciting with UV light, the as-prepared **DMCS-TPE** solid powders exhibit strong blue-green emission. After the grinding treatment using a pestle and a mortar, the emitting color of **DMCS-TPE** samples unexpectedly changes into yellowish green (Fig. 4b), indicating the obvious MFC feature. The mechanochromic effect of **DMCS-TPE** could be reverted to its original color by fuming with DCM vapor for 2 min. And when the fumed samples are re-ground, the fluorescence colors are again changed as the first grinding. The wavelength changes in solid-state emission could be repeated many times without fatigue, suggesting excellent reversibility in the switching processes (Fig. S11). PL spectra were used to monitor such naked-eye-visible fluorescence color changes under grinding and fuming stimuli. As depicted in Fig. 4a, the maximum emission wavelength of the as-prepared **DMCS-TPE** sample is 474 nm, and red-shifts to 531 nm in the ground powders, implying the PL spectrum of amorphous sample exhibits a significant 57 nm red-shift compared with the initial powders. Moreover, upon DCM fuming, its

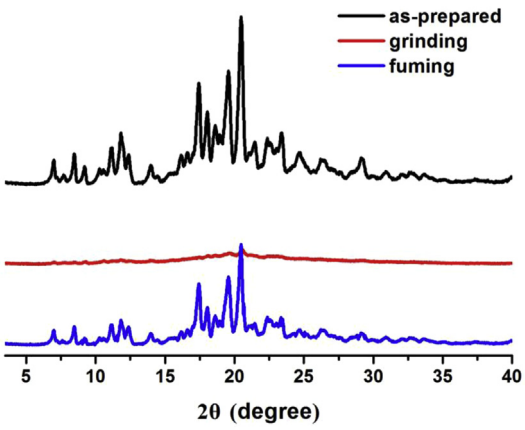

Fig. 5. XRD patterns of **DMCS-TPE** in different solid-states: as-prepared, grinding and fuming.

maximum emission wavelength can blue-shifted to the initial wavelength, which further suggests the reversibility of the mechanochromic fluorescence. Unexpectedly, the luminogen **DHCS-TPE** has no MFC properties. Grinding did not result in any change in the fluorescence color of **DHCS-TPE**, and the maximum emission wavelength remains almost unchanged and only the change of 1 nm is observed (Fig. S12).

To further understand the MFC behavior of **DHCS-TPE** and **DMCS-TPE**, the X-ray diffraction (XRD) measurements were carried out on their solid-state samples. As shown in Fig. 5, the XRD diffraction curves of the as-prepared **DMCS-TPE** solid powders display many sharp and intense reflections that are indicative of their regular crystalline nature. By sharp contrast, the ground solids show rather weak, broad, and diffused peaks, indicating disordered molecular packing or amorphous states. However, when fumed with DCM vapor, sharp diffractions, similar to those of the as-prepared solids, emerge again. These results show that after grinding, most of the ordered structures are disrupted. The grinding treatment can convert the crystalline phase to the amorphous state, and the fuming treatments can convert the amorphous phase to the crystalline state through molecular repacking, which realizes the reversible inter-conversion of mechanochromism. Therefore, the mechanochromism of **DMCS-TPE** is attributed to the transformations between the ordered crystalline and amorphous states. This is a general mechanism for many other mechanochromic compounds. In addition, the different MFC properties of the two compounds may be due to the electronic and steric effects of the peripheral substituents on the acceptor dicyanodistyrylbenzene axis with two *para*-hexyloxy and four *meta*-methoxy linkages. The large red-shifts of **DMCS-TPE** after grinding might be original from the conformational change and rotate to a position more parallel to the coplanar under external force, leading to extended conjugation and subsequent planar intramolecular charge transfer (PICT). This proposal could be evidenced by the UV-vis absorption spectra of as-prepared and ground samples (Fig. S13). It is obvious that the ground **DMCS-TPE** samples show a clear red-shift relative to that of as-prepared ones, indicating the extension of π-conjugation after grinding. Therefore, the planarization of the molecular conformation and subsequent PICT accounts for the MFC behavior of **DMCS-TPE**. However, for **DHCS-TPE**, the diffraction peaks in XRD pattern are coincident with those of the as-prepared powders (Fig. S14), confirming the fact that the green emission samples before and after grinding belong to the same crystalline morphology (Fig. S15). Moreover, the UV-vis absorption and PL spectra of its ground samples are almost the same as those of as-prepared ones, respectively (Figs. S12 and S16). Consequently, the color of the as-prepared and ground **DHCS-TPE** samples shows no changes. The no MFC behavior of **DHCS-TPE** might be due to its less twisted molecular conformation, which generates strong intermolecular forces and close packing. Therefore, the crystalline solid powders of **DHCS-TPE** possess higher lattice energy

and better structural stability than those of **DMCS-TPE**. The force of mechanical grinding cannot destroy the unit cell structure of **DHCS-TPE** crystals.

4. Conclusion

Two twisted donor–acceptor cruciform luminophores **DHCS-TPE** and **DMCS-TPE**, which were constructed by two π-conjugated electron-rich tetraphenylethene and electron-poor cyanostyryl intersecting at a central benzene core, have been designed and successfully prepared. The impact of molecular structure on photophysical properties was studied from the perspective of electronic and steric effects. It was found that the two cruciforms exhibited unique ICT emission, obvious AIE properties and strong solid-state fluorescence. The solid fluorescence quantum yield of **DHCS-TPE** and **DMCS-TPE** reach 0.913 and 0.424, respectively. More interestingly, the two compounds possess substituent-dependent MFC behavior. Owing to a more twisted molecular conformation, **DMCS-TPE** with four *meta*-methoxys on the acceptor dicyanodistyrylbenzene axis shows reversible high contrast MFC nature with large spectral shift of up to 57 nm, while the less twisted **DHCS-TPE** with two *para*-hexyloxys on the acceptor dicyanodistyrylbenzene axis has no MFC behavior. Due to the stronger intermolecular force and closer packing of **DHCS-TPE**, grinding of the crystalline solid powders doesn't affect their crystalline lattice, and thus grinding of **DHCS-TPE** crystals cannot lead to amorphization and mechanochromic luminescence. This study not only discloses a particular structure–property relationship between the luminescent polymorphs of organic luminophores, but also provides a perspective of the potential applications of these luminescence-switching polymorphs in the fields of optical displays and visual sensors for multiple external stimuli.

Acknowledgements

This work was financially supported by the National Natural Science Foundation of China (NNSFC, No. 21362027 and 21662028), Qinghai Province “High-end Innovative Thousand Talents Plan” (2017), the China Scholarship Council, and the Natural Science Foundation of QingHai Science & Technology Department (2016-ZJ-946Q).

Appendix A. Supplementary data

Supplementary data related to this article can be found at http://dx.doi.org/10.1016/j.dyepig.2018.04.021.

References

[1] (a) Caruso MM, Davis DA, Shen Q, Odom SA, Sottos NR, White SR, et al. Mechanically-induced chemical changes in polymeric materials. Chem Rev 2009;109:5755–98;
(b) Sagara Y, Kato T. Mechanically induced luminescence changes in molecular assemblies. Nat Chem 2009;1:605–10;
(c) Chi Z, Zhang X, Xu B, Zhou X, Ma C, Zhang Y, et al. Recent advances in organic mechanofluorochromic materials. Chem Soc Rev 2012;41:3878–96;
(d) Zhang X, Chi Z, Zhang Y, Liu S, Xu J. Recent advances in mechanochromic luminescent metal complexes. J Mater Chem C 2013;1:3376–90;
(e) Xue P, Ding J, Wang P, Lu R. Recent progress in the mechanochromism of phosphorescent organic molecules and metal complexes. J Mater Chem C 2016;4:6688–706.

[2] (a) Olson CE, Previte MJR, Fourkas JT. Efficient and robust multiphoton data storage in molecular glasses and highly crosslinked polymers. Nat Mater 2002;1:225–8;
(b) Hirata S, Watanabe T. Reversible thermoresponsive recording of fluorescent images (TRF). Adv Mater 2006;18:2725–9;
(c) Lim SJ, An BK, Jung SD, Chung MA, Park SY. Photoswitchable organic nanoparticles and a polymer film employing multifunctional molecules with enhanced fluorescence emission and bistable photochromism. Angew Chem Int Ed 2004;43:6346–50.

[3] (a) Pucci A, Ruggeri G. Mechanochromic polymer blends. J Mater Chem 2011;21:8282–91;
(b) Zhao N, Yang ZY, Lam JWY, Sung HHY, Xie N, Chen SJ, et al. Benzothiazolium-functionalized tetraphenylethene: an AIE luminogen with tunable solid-state emission. Chem Commun (J Chem Soc Sect D) 2012;48:8637–9;
(c) Park D-H, Hong J, Park IS, Lee CW, Kim J-M. A colorimetric hydrocarbon sensor employing a swelling-induced mechanochromic polydiacetylene. Adv Funct Mater 2014;24:5186–93;
(d) Tanioka M, Kamino S, Muranaka A, Ooyama Y, Ota H, Shirasaki Y, et al. Reversible near-infrared/blue mechanofluorochromism of aminobenzopyranoxanthene. J Am Chem Soc 2015;137:6436–9;
(e) Xue S, Qiu X, Sun Q, Yang W. Alkyl length effects on solid-state fluorescence and mechanochromic behavior of small organic luminophores. J Mater Chem C 2016;4:1568–78.

[4] (a) Kishimura A, Yamashita T, Yamaguchi K, Aida T. Rewritable phosphorescent paper by the control of competing kinetic and thermodynamic self-assembling events. Nat Mater 2005;4:546–9;
(b) Mutai T, Satou H, Araki K. Reproducible on-off switching of solid-state luminescence by controlling molecular packing through heat-mode interconversion. Nat Mater 2005;4:685–7;
(c) Sun H, Liu S, Lin W, Zhang KY, Lv W, Huang X, et al. Smart responsive phosphorescent materials for data recording and security protection. Nat Commun 2014;5:3601–9;
(d) Ito H, Saito T, Oshima N, Kitamura N, Ishizaka S, Hinatsu Y, et al. Reversible mechanochromic luminescence of $[(C_6F_5Au)_2(\mu\text{-}1,4\text{-diisocyanobenzene})]$. J Am Chem Soc 2008;130:10044–5.

[5] (a) Gong YY, Zhang YR, Yuan WZ, Sun JZ, Zhang YM. D–A solid emitter with crowded and remarkably twisted conformations exhibiting multifunctionality and multicolor mechanochromism. J Phys Chem C 2014;118:10998–1005;
(b) Yuan WZ, Gong YG, Chen SM, Shen XY, Lam JWY, Lu P, et al. Efficient solid emitters with aggregation-induced emission and intramolecular charge transfer characteristics: molecular design, synthesis, photophysical behaviors, and OLED application. Chem Mater 2012;24:1518–28;
(c) Gong YY, Tan YQ, Liu J, Lu P, Feng CF, Yuan WZ, et al. Twisted D–π–A solid emitters: efficient emission and high contrast mechanochromism. Chem Commun (J Chem Soc Sect D) 2013;49:4009–11.

[6] (a) Luo X, Zhao W, Shi J, Li C, Liu Z, Bo Z, et al. Reversible switching emissions of tetraphenylethene derivatives among multiple colors with solvent vapor, mechanical, and thermal stimuli. J Phys Chem C 2012;116:21967–72;
(b) Shen XY, Wang YJ, Zhao E, Yuan WZ, Liu Y, Lu P, et al. Effects of substitution with donor–acceptor groups on the properties of tetraphenylethene trimer: aggregation-induced emission, solvatochromism, and mechanochromism. J Phys Chem C 2013;117:7334–47;
(c) Peng Z, Huang K, Tao Y, Li X, Zhang L, Lu P, et al. Turning on the solid emission from non-emissive 2-aryl-3-cyanobenzofurans by tethering tetraphenylethene for green electroluminescence. Mater Chem Front 2017;1:1858–65;
(d) Zhang X, Chi Z, Xu B, Chen C, Zhou X, Zhang Y, et al. End-group effects of piezofluorochromic aggregation-induced enhanced emission compounds containing distyrylanthracene. J Mater Chem 2012;22:18505–13;
(e) Ma C, Xu B, Xie G, He J, Zhou X, Peng B, et al. An AIE-active luminophore with tunable and remarkable fluorescence switching based on the piezo and protonation–deprotonation control. Chem Commun (J Chem Soc Sect D) 2014;50:7374–7;
(f) Lu Q, Li X, Li J, Yang Z, Xu B, Chi Z, et al. Influence of cyano groups on the properties of piezofluorochromic aggregation-induced emission enhancement compounds derived from tetraphenylvinyl-capped ethane. J Mater Chem C 2015;3:1225–34;
(g) Xu B, Xie M, He J, Xu B, Chi Z, Tian W, et al. An aggregation-induced emission luminophore with multi-stimuli single- and two-photon fluorescence switching and large two-photon absorption cross section. Chem Commun (J Chem Soc Sect D) 2013;49:273–5.

[7] (a) Zhang X, Chi Z, Xu B, Jiang L, Zhou X, Zhang Y, et al. Multifunctional organic fluorescent materials derived from 9,10-distyrylanthracene with alkoxyl endgroups of various lengths. Chem Commun (J Chem Soc Sect D) 2012;48:10895–7;
(b) Li H, Zhang X, Chi Z, Xu B, Zhou W, Liu S, et al. New thermally stable piezofluorochromic aggregation-induced emission compounds. Org Lett 2011;13:556–9;
(c) Zhang X, Chi Z, Li H, Xu B, Li X, Zhou W, et al. Piezofluorochromism of an aggregation-induced emission compound derived from tetraphenylethylene. Chem Asian J 2011;6:808–11;
(d) Dong Y, Xu B, Zhang J, Tan X, Wang L, Chen J, et al. Piezochromic luminescence based on the molecular aggregation of 9,10-bis((*E*)-2-(pyrid-2-yl)vinyl)anthracene. Angew Chem Int Ed 2012;51:10782–5;
(e) Dong Y, Zhang J, Tan X, Wang L, Chen J, Li B, et al. Multi-stimuli responsive fluorescence switching: the reversible piezochromism and protonation effect of a divinylanthracene derivative. J Mater Chem C 2013;1:7554–9;
(f) Sagara Y, Yamane S, Mutai T, Araki K, Kato T. A Stimuli-responsive, photoluminescent, anthracene-Based liquid crystal: emission color determined by thermal and mechanical processes. Adv Funct Mater 2009;19:1869–75;
(g) Liu W, Wang Y, Sun M, Zhang D, Zheng M, Yang W. Alkoxy-position effects on piezofluorochromism and aggregation-induced emission of 9,10-bis(alkoxystyryl) anthracenes. Chem Commun (J Chem Soc Sect D) 2013;49:6042–4;
(h) Bu L, Sun M, Zhang D, Liu W, Wang Y, Zheng M, et al. Solid-state fluorescence properties and reversible piezochromic luminescence of aggregation-induced emission-active 9,10-bis[(9,9-dialkylfluorene-2-yl)vinyl]anthracenes. J Mater Chem C 2013;1:2028–35.

[8] (a) Yuan WZ, Tan Y, Gong Y, Lu P, Lam JWY, Shen XY, et al. Synergy between twisted conformation and effective intermolecular interactions: strategy for efficient mechanochromic luminogens with high contrast. Adv Mater 2013;25:2837–43;
(b) Zhang G, Sun J, Xue P, Zhang Z, Gong P, Peng J, et al. Phenothiazine modified triphenylacrylonitrile derivates: AIE and mechanochromism tuned by molecular

conformation. J Mater Chem C 2015;3:2925–32.
[9] (a) Zhang G, Lu J, Sabat M, Fraser CL. Polymorphism and reversible mechanochromic luminescence for solid-state difluoroboron avobenzone. J Am Chem Soc 2010;132:2160–2;
(b) Zhang G, Singer JP, Kooi SE, Evans RE, Thomas EL, Fraser CL. Reversible solid-state mechanochromic fluorescence from a boron lipid dye. J Mater Chem 2011;21:8295–9;
(c) Yoshii R, Suenaga K, Tanaka K, Chujo Y. Mechanofluorochromic materials based on aggregation-induced emission-active boron ketoiminates: regulation of the direction of the emission color changes. Chem Eur J 2015;21:7231–7;
(d) Yamaguchi M, Ito S, Hirose A, Tanaka K, Chujo Y. Modulation of sensitivity to mechanical stimulus in mechanofluorochromic properties by altering substituent positions in solid-state emissive diiodo boron diiminates. J Mater Chem C 2016;4:5314–9;
(e) Zhang Z, Wu Z, Sun J, Yao B, Zhang G, Xue P, et al. Mechanofluorochromic properties of β-iminoenolate boron complexes tuned by the electronic effects of terminal phenothiazine and phenothiazine-*S,S*-dioxide. J Mater Chem C 2015;3:4921–32;
(f) Wang X, Liu Q, Yan H, Liu Z, Yao M, Zhang Q, et al. Piezochromic luminescence behaviors of two new benzothiazole–enamido boron difluoride complexes: intra- and inter-molecular effects induced by hydrostatic compression. Chem Commun (J Chem Soc Sect D) 2015;51:7497–500;
(g) Galer P, Korošec RC, Vidmar M, Šket B. Crystal structures and emission properties of the BF_2 complex 1-phenyl-3-(3,5-dimethoxyphenyl)-propane-1,3-dione: multiple chromisms, aggregation- or crystallization-induced emission, and the self-assembly effect. J Am Chem Soc 2014;136:7383–94.
[10] (a) Zhou L, Xu D, Gao H, Han A, Liu X, Zhang C, et al. Triphenylamine functionalized β-Ketoiminate boron complex exhibiting aggregation-induced emission and mechanofluorochromism. Dyes Pigments 2017;137:200–7;
(b) Gao H, Xu D, Liu X, Han A, Zhou L, Zhang C, et al. Tetraphenylethene-based β-diketonate boron complex: efficient aggregation-induced emission and high contrast mechanofluorochromism. Dyes Pigments 2017;139:157–65;
(c) Zhou L, Xu D, Gao H, Han A, Yang Y, Zhang C, et al. Effects of cyano groups on the properties of thiazole-based β-ketoiminate boron complexes: aggregation-induced emission and mechanofluorochromism. RSC Adv 2016;6:69560–8;
(d) Gao H, Xu D, Wang Y, Wang Y, Liu X, Han A, et al. Effects of alkyl chain length on aggregation-induced emission, self-assembly and mechanofluorochromism of tetraphenylethene modified multifunctional β-diketonate boron complexes. Dyes Pigments 2018;150:59–66.
[11] (a) Liu J, Lam JWY, Tang BZ. Acetylenic polymers: syntheses, structures, and functions. Chem Rev 2009;109:5799–867;
(b) Hong YN, Lam JWY, Tang BZ. Aggregation-induced emission. Chem Soc Rev 2011;40:5361–88;
(c) Sasaki S, Drummen GPC, Konishiac G. Recent advances in twisted intramolecular charge transfer (TICT) fluorescence and related phenomena in materials chemistry. J Mater Chem C 2016;4:2731–43.
[12] (a) Luo J, Xie Z, Lam JWY, Cheng L, Chen H, Qiu C, et al. Aggregation-induced emission of 1-methyl-1,2,3,4,5-pentaphenylsilole. Chem Commun (J Chem Soc Sect D) 2001:1740–1;
(b) Mei J, Leung NLC, Kwok RTK, Lam JWY, Tang BZ. Aggregation-induced emission: together we shine, united we soar!. Chem Rev 2015;115:11718–940.
[13] (a) Han T, Zhang Y, Feng X, Lin Z, Tong B, Shi J, et al. Reversible and hydrogen bonding-assisted piezochromic luminescence for solid-state tetraaryl-buta-1,3-diene. Chem Commun (J Chem Soc Sect D) 2013;49:7049–51;
(b) Tian H, Wang P, Liu J, Duan Y, Dong YQ. Construction of a tetraphenylethene derivative exhibiting high contrast and multicolored emission switching. J Mater Chem C 2017;5:12785–91.
[14] (a) Zucchero AJ, Wilson JN, Bunz UHF. Cruciforms as functional fluorophores: response to protons and selected metal ions. J Am Chem Soc 2006;128:11872–81;
(b) Sun J, Lv X, Wang P, Zhang Y, Dai Y, Wu Q, et al. A donor–acceptor cruciform π-system: high contrast mechanochromic properties and multicolour electrochromic behavior. J Mater Chem C 2014;2:5365–71;
(c) Liu W, Wang J, Gao Y, Sun Q, Xue S, Yang W. 2,6,9,10-Tetra(*p*-dibutylaminostyryl)anthracene as a multifunctional fluorescent cruciform dye. J Mater Chem C 2014;2:9028–34.
[15] (a) Xie Z, Yang B, Li F, Cheng G, Liu L, Yang G, et al. Cross dipole stacking in the crystal of distyrylbenzene derivative: the approach toward high solid-state luminescence efficiency. J Am Chem Soc 2005;127:14152–3;
(c) Sun J, Zhong H, Xu E, Zeng D, Zhang J, Xu H, et al. An X-shaped solution-processible oligomer having an anthracene unit as a core: a new organic light-emitting material with high thermostability and efficiency. Org Electron 2010;11:74–80;
(d) Xue S, Yao L, Liu S, Gu C, Shen F, Li W, et al. Simultaneous enhancement of the Carrier mobility and luminous efficiency through thermal annealing a molecular glass material and device. J Mater Chem 2012;22:21502–6.
[16] (a) Zhang H, Guo E, Zhang Y, Ren P, Yang W. Donor－acceptor-substituted anthracene-centered cruciforms: synthesis, enhanced two-photon absorptions, and spatially separated frontier molecular orbitals. Chem Mater 2009;21:5125–9;
(b) He F, Tian L, Tian X, Xu H, Wang Y, Xie W, et al. Diphenylamine-substituted cruciform oligo(phenylene vinylene): enhanced one- and two-photon excited fluorescence in the solid state. Adv Funct Mater 2007;17:1551–7.
[17] Xue S, Liu S, He F, Yao L, Gu C, Xu H, et al. Chemistry and materials based on 5,5′-bibenzo[c][1,2,5]thiadiazole. Chem Commun (J Chem Soc Sect D) 2013;49:5730–2.
[18] Xu B, Chi Z, Zhang J, Zhang X, Li H, Li X, et al. Piezofluorochromic and aggregation-induced-emission compounds containing triphenylethylene and tetraphenylethylene moieties. Chem Asian J 2011;6:1470–8.
[19] Sun J, Dai Y, Ouyang M, Zhang Y, Zhan L, Zhang C. Unique torsional cruciform π-architectures composed of donor and acceptor axes exhibiting mechanochromic and electrochromic properties. J Mater Chem C 2015;3:3356–63.
[20] (a) Yang J-S, Liau K-L, Wang C-M, Hwang C-Y. Substituent-dependent photo-induced intramolecular charge transfer in *N*-aryl-substituted *trans*-4-aminostilbenes. J Am Chem Soc 2004;126:12325–35;
(b) Liu X, Zhang X, Lu R, Xue P, Xu D, Zhou H. Low-dimensional nanostructures fabricated from bis(dioxaborine)carbazole derivatives as fluorescent chemosensors for detecting organic amine vapors. J Mater Chem 2011;21:8756–65.
[21] Lippert EZ. Dipolmoment und Elektronenstruktur von angeregten Molekülen Z. Naturforsch., A Phys Sci 1955;10:541–5.
[22] Mataga N, Kaifu Y, Koizumi M. Solvent effects upon fluorescence spectra and the dipolemoments of excited molecules. Bull Chem Soc Jpn 1956;29:465–70.
[23] Sun W, Zhou C, Xu C-H, Zhang Y-Q, Li Z-X, Fang C-J, et al. Intramolecular charge transfer in 5-methoxy-2-(2-pyridyl)thiazole-derived fluorescent molecules with different acceptor or donor substituents. J Phys Chem 2009;113:8635–46.